Computers and Mathematics with Applications 64 (2012) 856–868

Contents lists available at SciVerse ScienceDirect

Computers and Mathematics with Applications

journal homepage: www.elsevier.com/locate/camwa

Singularity avoidance of a six degree of freedom three dimensional redundant planar manipulator

Samer Yahya [a,*], M. Moghavvemi [a], Haider A.F. Mohamed [b]

[a] Center of Research in Applied Electronics (CRAE), University of Malaya, 50603, Malaysia
[b] Department of Electrical & Electronic Engineering The University of Nottingham Malaysia Campus, Malaysia

ARTICLE INFO

Keywords:
Planar manipulator
Redundant manipulator
Kinematics
Singularity avoidance
Manipulability

ABSTRACT

This paper focuses on the improvement of singularity avoidance of three dimensional planar redundant manipulators by increasing its degrees of freedom without increasing the number of motors controlling the manipulator. Consequently, the method to build a three dimensional planar manipulator with six-degrees of freedom using three motors instead of six is discussed in detail. A comparison of the manipulability index values for the proposed manipulator is made with the manipulability index values of PUMA arm to demonstrate the effectiveness of using the proposed manipulator for singularity avoidance.

1. Introduction

A robotic system is considered kinematically redundant when it possesses more degrees of freedom than those required to execute a given task [1,2]. Usually, the kinematics of non redundant robots is solved by deriving analytical solutions for several manipulator configurations [3]. When a manipulator is redundant, it is anticipated that the inverse kinematics has infinite solutions. This implies that, for a given location of the manipulator's end-effectors, it is possible to induce self-motion in the structure without changing its location [4,5]. Therefore, classical methods cannot be used to solve their inverse kinematics. Many previous investigations have focused on the redundancy resolution of this type of manipulator, based on the manipulator's Jacobian pseudoinverse.

A redundant manipulator with a degree-of-redundancy is well suited to a multiple criteria problem on top of the basic motion task, such as obstacle avoidance, singularity avoidance, and torque minimization. For the multiple task problems, the cost function should be determined in accordance with the additional task having higher priority.

A considerable portion of the workspace of a robot manipulator is occupied by singularities. These regions correspond to robot configurations, at which the joint rates necessary to achieve an end-effector motion along one or more directions are extremely high. In other words, in the neighborhood of singular postures, even a small change in Δt requires a large change in $\Delta\theta$, which is practically unfeasible and hazardous [6]. When planning robotic applications, a common problem is the need to avoid singular arm configurations, where the robot performance is seriously degraded in order to be able to move and apply uniform forces in all directions, the manipulator must stay as far away as possible from singularities [7].

Consider a manipulator with n degrees of freedom, whose joint variables are denoted by $\theta_i = \theta_i(t)$; $i = 1, 2, \ldots, n$. A manipulation variable describing the robot's task is also defined as an m component vector $x_j = x_j(t)$; $j = 1, 2, \ldots, m$. Then, θ and x are related by the forward kinematic transformation:

$$x = f(\theta). \tag{1}$$

* Corresponding author.
E-mail address: smryahya@siswa.um.edu.my (S. Yahya).

0898-1221/$ – see front matter © 2011 Elsevier Ltd. All rights reserved.
doi:10.1016/j.camwa.2011.12.073

By differentiating this equation with respect to time and defining $J = df/d\theta$, the following equation is obtained:

$$\dot{x} = J\dot{\theta}. \tag{2}$$

If J is a square matrix ($m = n$), and has a rank equal to m (full rank), then joint velocities required to achieve the desired end-effector velocity will be unique and can be evaluated by:

$$\dot{\theta} = J^{-1}\dot{x}. \tag{3}$$

But in the control of redundant robots with ($m > n$), the vast majority of research involved resolution through the use of the pseudoinverse J^+ of the Jacobian matrix J [8]:

$$\dot{\theta} = J^{+}\dot{x}. \tag{4}$$

This solution minimizes $\left\|\dot{\theta}\right\|^2$. Because of this minimizing property, the early hope of [9] shows that singularities will automatically be avoided. It is also shown that without modification, this approach does not avoid singularity [10,11]. Moreover, [12] pointed out that it does not produce cyclic behavior, which denotes a serious practical problem.

For these reasons, another component belonging to the null space of the Jacobian has to be added to the pseudoinverse solution to realize the secondary objective function. The basic redundancy resolution scheme is the gradient projection method [13], by which the general solution is written as:

$$\dot{\theta} = J^{+}\dot{x} + (I_n - J^{+}J)z \tag{5}$$

where J^+ denotes the pseudo-inverse of J and it is defined in the following manner

$$J^{+} = J^{T}(JJ^{T})^{-1} \tag{6}$$

such that

$$JJ^{T} = I_m. \tag{7}$$

The pseudo-inverse defined by Eq. (6) satisfies the following conditions [14,15]:

$$JJ^{T}J = J \tag{8}$$

$$J^{+}JJ^{+} = J^{+} \tag{9}$$

$$(J^{+}J)^{T} = J^{+}J \tag{10}$$

$$(JJ^{+})^{T} = JJ^{+}. \tag{11}$$

In addition, the matrix $(I_n - J^{+}J)$ satisfies the following useful properties:

$$(I_n - J^{+}J)(I_n - J^{+}J) = (I_n - J^{+}J) \tag{12}$$

$$J(I_n - J^{+}J) = 0 \tag{13}$$

$$(I_n - J^{+}J)^{T} = (I_n - J^{+}J) \tag{14}$$

$$(I_n - J^{+}J)J^{+} = 0. \tag{15}$$

In Eq. (5), z is an arbitrary (n*1) vector in the $\dot{\theta}$ space. The second term on the right-hand side of this equation belongs to the null space of J, and it corresponds to a self-motion of the joints that does not move the end-effector. This term, which is called a homogeneous solution or an optimization term, can be used to optimize a desired function $\varphi\ (\theta)$ [10]. In fact, taking $z = \alpha\nabla\varphi$ where $\nabla\varphi$ is the gradient of this function with respect to θ minimizes the function $\varphi\ (\theta)$ when $\alpha < 0$ and maximizes when $\alpha > 0$. Eq. (5) is rewritten as:

$$\dot{\theta} = J^{+}\dot{x} + \alpha(I_n - J^{+}J)\nabla\varphi \tag{16}$$

with

$$\nabla\varphi = \begin{bmatrix} \dfrac{\partial\varphi}{\partial\theta_1} & \cdots & \dfrac{\partial\varphi}{\partial\theta_n} \end{bmatrix}. \tag{17}$$

The value of α allows a trade-off between the minimization and the optimization of $\varphi\ (\theta)$. As mentioned earlier, the secondary performance criteria can be optimized, and $\varphi\ (\theta)$ is used for minimizing the norm of the joint velocities, avoiding obstacles, singular configurations, and joints limits, or minimizing driving joint torques.

Clearly, the effect of singularity is experienced not only at the singular configuration but also in its neighborhood, because the manipulating ability of the robot in this region gets severely restricted [16]. For this reason, it is important to be able to characterize the distance from singularities through suitable measures; these can then be exploited to counteract

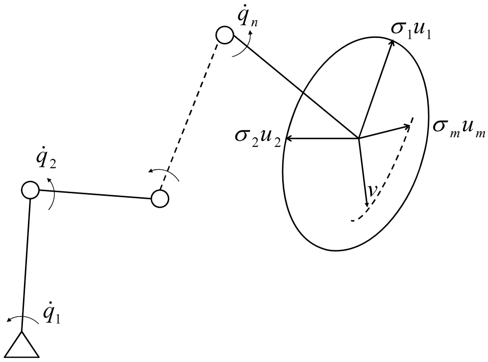

Fig. 1. Manipulability ellipsoid [19].

undesirable effects. During the past three decades, many researchers have suggested various methods to fully utilize the redundancy of robots.

One of the earliest and most recognized Jacobian based manipulator performance measures were explained in [17]. This measure is the manipulability measure, where

$$M = \sqrt{\det(JJ^T)}. \tag{18}$$

Let the singular decomposition of J be [18]:

$$J = U \sum V^T \tag{19}$$

where $U \in R^{m\times m}$and $V \in R^{n\times n}$ are orthogonal matrices and

$$\Sigma = \left[\begin{array}{cccc|c} \sigma_1 & & & 0 & \\ & \sigma_2 & & & 0 \\ & & . & & \\ 0 & & & \sigma_m & \end{array}\right] \in R^{m\times n} \tag{20}$$

with

$$\sigma_1 \geq \sigma_2 \geq \cdots \geq \sigma_m \geq 0. \tag{21}$$

The scalars $\sigma_1, \sigma_2, \ldots, \sigma_m$ are called singular values of J, and they are equal to the m larger values of the n roots $\{\sqrt{\lambda_i}, i = 1, 2, \ldots, n\}$, where λ_i $(i = 1, 2, \ldots, n)$ are the eigenvalues of the matrix J^TJ [19]. Further, let u_i be the ith column vector of U. Then the principal axes of the manipulability ellipsoid are $\sigma_1u_1, \sigma_2u_2, \ldots, \sigma_m u_m$; see Fig. 1. In the direction of the major axis of the ellipsoid, the end-effector moves at high speed. On the other hand, in the direction of the minor axis, the end-effector moves at low speed, and if the ellipsoid is almost a sphere, the end-effector uniformly moves in all directions. A larger ellipsoid allows faster end-effector movements.

The number of nonzero singular value is

$$r = \text{rank}(J). \tag{22}$$

Since U and V are orthogonal, they satisfy

$$UU^T = U^TU = I_m \tag{23}$$

$$VV^T = V^TV = I_n. \tag{24}$$

Let us consider the meaning of the singular value decomposition of J in relation to the linear transformation $y = Jx$. Letting $y_U = U^Ty$ and $x_V = V^Tx$, from Eq. (19) we have

$$y_U = \Sigma x_V. \tag{25}$$

This implies that the transformation from x to y can be decomposed into three consecutive transformations: the orthogonal transformation from x to x_V by V^T, which does not change length; from x_V to y_U, in which the ith element of x_V is multiplied by σi and becomes the ith element of y_U without changing its direction; the orthogonal transform from y_U to y by U, which does not change its length. Therefore, the singular value decomposition highlights a basic property of linear transformation [19].

A scheme to obtain the singular value decomposition follows. First, we calculate the singular values by:

$$\sigma_i = \sqrt{\lambda_i}, \quad i = 1, 2, \ldots, n. \tag{26}$$

Next we obtain U and V. We define a diagonal matrix $\sum_r$ using r nonzero singular values by:

$$\Sigma_r = \begin{bmatrix} \sigma_1 & & 0 \\ & \ddots & \\ 0 & & \sigma_r \end{bmatrix}. \tag{27}$$

This is the $r \times r$ principal minor of $\sum$. We let the ith row vectors of U and V be u_i and v_i respectively, and let

$$U_r = [u_1, u_2, \ldots, u_r] \tag{28}$$

and

$$V_r = [v_1, v_2, \ldots, v_r]. \tag{29}$$

Then from Eq. (19):

$$J = U_r \sum_r V_r^T. \tag{30}$$

Also from Eqs. (23) and (24):

$$U_r^T U_r = I_r \tag{31}$$

$$V_r^T V_r = I_r. \tag{32}$$

Hence we have

$$J^T J V_r = V_r \Sigma_r^2 \tag{33}$$

$$U_r = J V_r \Sigma_r^{-1}. \tag{34}$$

Since Eq. (33) can be decomposed into:

$$J^T J v_i = v_i \sigma_i^2, \quad i = 1, 2, \ldots, r. \tag{35}$$

We see that v_i is the eigenvector of unit length for eigenvalue λ_i of $J^T J$. Then we can determine V_r from the eigenvectors of $J^T J$ for the eigenvalues $\lambda_1, \lambda_2, \ldots, \lambda_r$. The part of V other than V_r, which consists of the vectors $v_{r+1}, v_{r+2}, \ldots, v_n$, is arbitrary, as long as it satisfies Eq. (24). From the obtained V we can determine U_r using Eq. (34) and the other part of U by Eq. (23).

Because of the singular configuration the robotic manipulator reaches during certain task execution is one of the challenges faced by the researchers; avoidance of the singular configurations is studied here. The manipulability values have been calculated for a proposed manipulator, and the results are compared to the manipulability values of PUMA manipulator in all the workspace of the manipulators to show the effectiveness of using the proposed manipulator for singularity avoidance.

2. Kinematics of the proposed manipulator

Consider the six degrees of freedom for the three dimensional planar manipulator shown in Fig. 2, where l_i denotes the i-th link, θ_i denotes the i-th joint angle, and (x_{tp}, y_{tp}, z_{tp}) is the target point. To find the position coordinates (x_{tp}, y_{tp}, z_{tp}), the following equations can be used:

$$\begin{aligned} x_{tp} = {} & \cos[\theta_1](l_1 \cos[\theta_2] + l_2 \cos[\theta_2 + \theta_3] + l_3 \cos[\theta_2 + \theta_3 + \theta_4] + l_4 \cos[\theta_2 + \theta_3 \\ & + \theta_4 + \theta_5] + l_5 \cos[\theta_2 + \theta_3 + \theta_4 + \theta_5 + \theta_6]) \end{aligned} \tag{36}$$

$$\begin{aligned} y_{tp} = {} & \sin[\theta_1](l_1 \cos[\theta_2] + l_2 \cos[\theta_2 + \theta_3] + l_3 \cos[\theta_2 + \theta_3 + \theta_4] + l_4 \cos[\theta_2 + \theta_3 \\ & + \theta_4 + \theta_5] + l_5 \cos[\theta_2 + \theta_3 + \theta_4 + \theta_5 + \theta_6]) \end{aligned} \tag{37}$$

$$\begin{aligned} z_{tp} = {} & (l_1 \sin[\theta_2] + l_2 \sin[\theta_2 + \theta_3] + l_3 \sin[\theta_2 + \theta_3 + \theta_4] + l_4 \sin[\theta_2 + \theta_3 + \theta_4 \\ & + \theta_5] + l_5 \sin[\theta_2 + \theta_3 + \theta_4 + \theta_5 + \theta_6]). \end{aligned} \tag{38}$$

As long as the manipulability measure, M of manipulator is based on the Jacobian matrix J, the Jacobian matrix of the manipulator is calculated as:

$$J = \begin{bmatrix} \frac{\partial x_{tp}}{\partial \theta_1} & \frac{\partial x_{tp}}{\partial \theta_2} & \frac{\partial x_{tp}}{\partial \theta_3} & \frac{\partial x_{tp}}{\partial \theta_4} & \frac{\partial x_{tp}}{\partial \theta_5} & \frac{\partial x_{tp}}{\partial \theta_6} \\ \frac{\partial y_{tp}}{\partial \theta_1} & \frac{\partial y_{tp}}{\partial \theta_2} & \frac{\partial y_{tp}}{\partial \theta_3} & \frac{\partial y_{tp}}{\partial \theta_4} & \frac{\partial y_{tp}}{\partial \theta_5} & \frac{\partial y_{tp}}{\partial \theta_6} \\ \frac{\partial z_{tp}}{\partial \theta_1} & \frac{\partial z_{tp}}{\partial \theta_2} & \frac{\partial z_{tp}}{\partial \theta_3} & \frac{\partial z_{tp}}{\partial \theta_4} & \frac{\partial z_{tp}}{\partial \theta_5} & \frac{\partial z_{tp}}{\partial \theta_6} \end{bmatrix}. \tag{39}$$

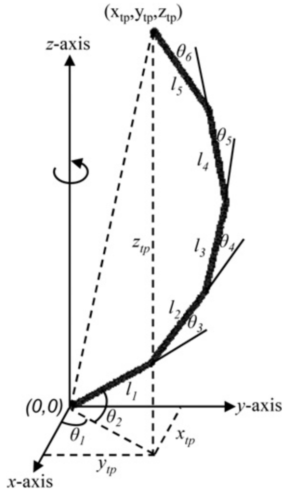

Fig. 2. A three dimensional planar redundant manipulator configuration.

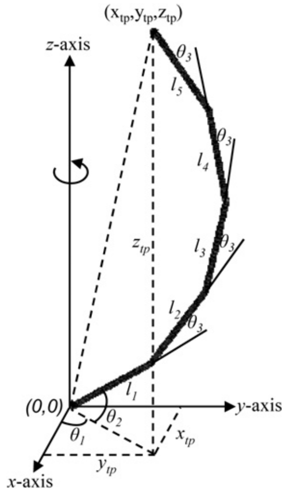

Fig. 3. A three dimensional planar redundant manipulator configuration using the method of Ref. [20].

Improving the ability of the manipulator in the singularity avoidance, the method in [20] is used. This method considers the angles between the adjacent links as equal, which means $\theta_3 = \theta_4 = \theta_5 = \theta_6$. Fig. 3 shows the configuration of the new manipulator.

For the proposed manipulator (Fig. 4), as long as the angles ($\theta_3, \theta_4, \theta_5, \theta_6$) are equal, there is no need for a motor for each angle, greatly decreasing the weight of the manipulator. This means that instead of using six motors to control the manipulator, only three is required. The first motor is used to control the first joint angle (θ_1), and the second motor is used to control the second joint angle (θ_2), as shown in Fig. 5.

The third motor is used to control the joint angles ($\theta_3, \theta_4, \theta_5, \theta_6$), and it is connected to the second link using a worm gear. Controlling the second motor means controlling the angle between the first link and the second link i.e. the angle θ_3. Fig. 6 shows the second joint angle and as with the first link, the second link and the gear (wheel) are fixed; rotating the worm will rotate the gear and the second link simultaneously by the angle θ_3. Transferring this movement to the next link requires a planetary gear, shown in Fig. 6. This planetary gear consists of two bevel gears and an arm. The first bevel gear is fixed to the first link, while the arm is fixed to the wheel gear and the second link, which means that rotating the wheel gear will result in the rotation of the arm with the same angular velocity of the wheel gear, which in turn will rotate the second bevel gear around the first fixed bevel gear.

The mechanism of the third link is shown in Fig. 7. It is similar to the one used in the second link; the only difference is instead of using worm as a driver and the wheel gear as the component being driven, two bevel gears are used. The first bevel gear (driver) is fixed to the second bevel gear of the previous link, i.e. the first bevel gear of Fig. 7 is fixed to the second bevel gear of Fig. 6. Because the second bevel gear of the third link is fixed to the third link, rotating the first bevel gear of the link will also rotate the second bevel gear, which will in turn rotate the third link. This movement can be translated to

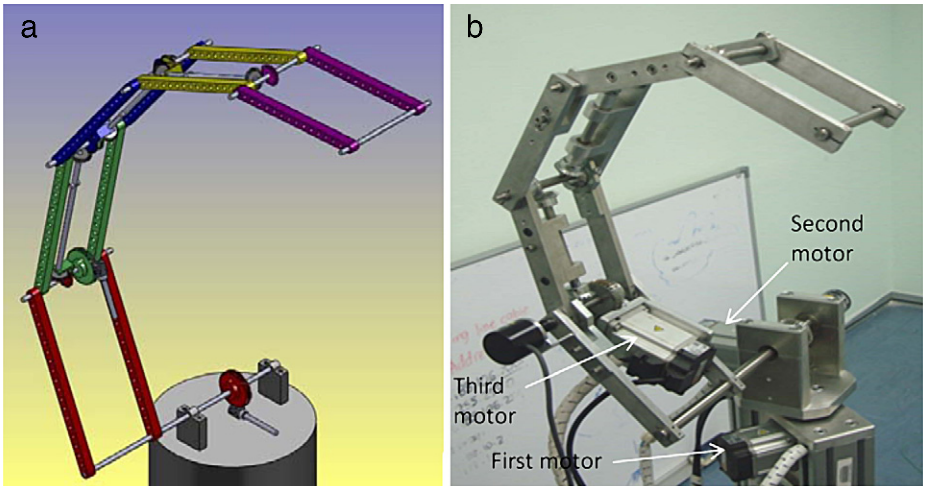

Fig. 4. The manipulator used in experiments. (a) The draft of the manipulator using the SolidWorks software; (b) the mechanical design of the manipulator.

the next link the same way the rotation was translated from the second link to the third link. In other words, a planetary gear is used to translate the rotation to the next link, as shown in Fig. 7.

This method has two advantages, namely, the usage of three motors instead of six, which reduces the number of motors controlling the manipulator, reducing the complexity of manipulator control, while also increasing the ability of the manipulator to avoid singularity, as will be explained later in this paper.

Calculating the manipulability measure for the new manipulator uses equations (39) and (18), detailed below:

$$\begin{aligned} M = \mathrm{sqrt}\Bigg(& \sin^2(\theta_3)\Big(l_1\cos(\theta_2) + l_2\cos(\theta_2+\theta_3) + l_3\cos(\theta_2+2\theta_3) + l_4\cos(\theta_2+3\theta_3) \\ & + l_5\cos(\theta_2+4\theta_3)\Big)^2 (l_1^2(8l_3^2\cos^2(\theta_3) + 2l_2(2l_3\cos(\theta_3) + l_4(2\cos(2\theta_3)+1) + 2l_5(\cos(\theta_3)+\cos(3\theta_3))) \\ & + 12l_4^2\cos(2\theta_3) + 6l_4^2\cos(4\theta_3) + 24l_5^2\cos(2\theta_3) + 16l_5^2\cos(4\theta_3) + 8l_5^2\cos(6\theta_3) \\ & + 8l_3\cos(\theta_3)(l_4(2\cos(2\theta_3)+1) + 2l_5(\cos(\theta_3)+\cos(3\theta_3))) \\ & + 36l_4l_5\cos(\theta_3) + 24l_4l_5\cos(3\theta_3) + 12l_4l_5\cos(5\theta_3) + l_2^2 + 9l_4^2 + 16l_5^2) \\ & + 2l_1(l_3(16l_5^2\cos^2(\theta_3)\cos(2\theta_3) + l_4^2(2\cos(2\theta_3)+1) + 2l_5l_4(3\cos(\theta_3)+2\cos(3\theta_3))) \\ & + 2l_4l_5^2(\cos(\theta_3)+\cos(3\theta_3)) + l_2(2l_3^2\cos(\theta_3) + l_3(l_4(4\cos(2\theta_3)+3) + 2l_5(3\cos(\theta_3)+2\cos(3\theta_3))) \\ & + 2(2l_4^2(2\cos(\theta_3)+\cos(3\theta_3)) + l_5l_4(8\cos(2\theta_3)+4\cos(4\theta_3)+5) + 3l_5^2(3\cos(\theta_3)+2\cos(3\theta_3) \\ & + \cos(5\theta_3))))) + 2l_2^2(8l_4^2\cos^2(\theta_3) + 2l_3(2l_4\cos(\theta_3) + l_5(2\cos(2\theta_3)+1)) \\ & + 3l_5^2(2\cos(2\theta_3)+1)^2 + 8l_4l_5(2\cos(\theta_3)+\cos(3\theta_3)) + l_3^2) \\ & + 12l_3^2l_5^2\cos(2\theta_3) + 12l_3l_4l_5^2\cos(\theta_3) + 4l_2(l_4l_5^2(2\cos(2\theta_3)+1) \\ & + l_3(2l_4^2\cos(\theta_3) + l_5l_4(4\cos(2\theta_3)+3) + 4l_5^2(2\cos(\theta_3)+\cos(3\theta_3)))) \\ & + 12l_3^2l_4l_5\cos(\theta_3) + 3l_3^2l_4^2 + 12l_3^2l_5^2 + 4l_4^2l_5^2)\Bigg). \end{aligned} \tag{40}$$

This equation proves that the first joint angle does not have a big impact on the value of manipulability. The manipulability values for the whole workspace for our manipulator are calculated using Eq. (40), and for our manipulator, $l_1 = 19, l_2 = 18, l_3 = 17, l_4 = 16, l_5 = 15$, with all the dimensions in cm. To be able to draw the manipulability values for the entire workspace, we need to know the values of the joint angles, which lead the manipulator to its minimum and maximum reach. Calculating these angles requires the determination of s, the distance between the end-effector and the origin:

$$s = \sqrt{x_{tp}^2 + y_{tp}^2 + z_{tp}^2}. \tag{41}$$

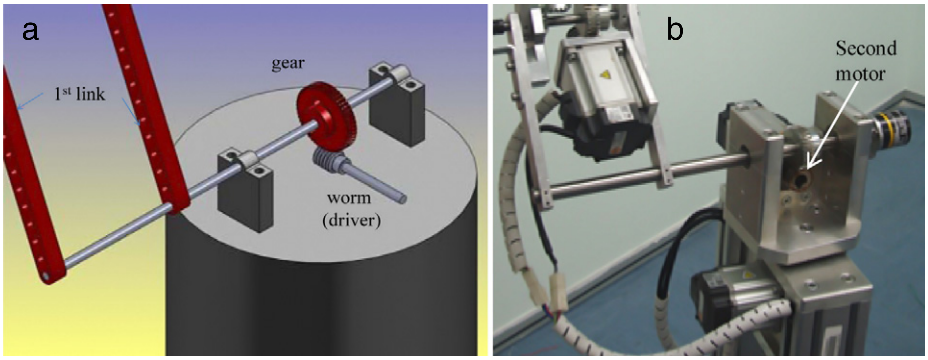

Fig. 5. The design of the second joint angle (first link with second motor) of the manipulator. (a) The draft of the second joint angle using the SolidWorks software; (b) the mechanical design of the second joint angle.

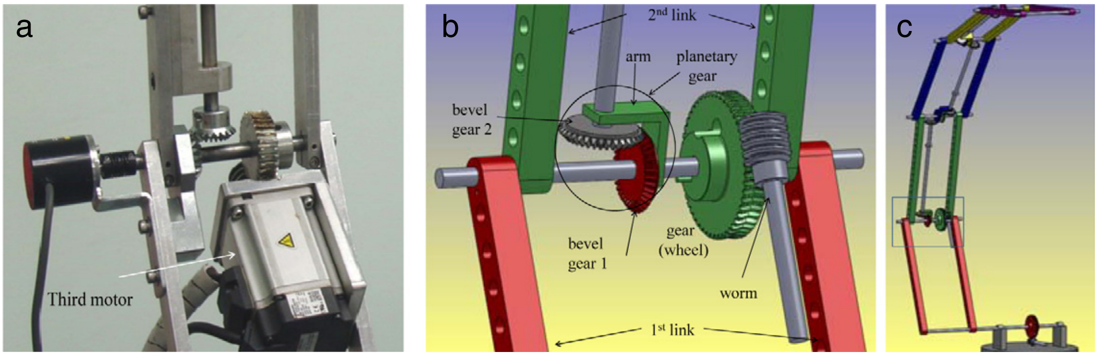

Fig. 6. The design of the third joint angle (second link with third motor) of the manipulator. (a) The mechanical design of the third joint angle; (b) the draft of the third joint angle using the SolidWorks software; (c) the draft of the entire manipulator using the SolidWorks software.

Substitute Eqs. (36)–(38) in Eq. (41), and we get

$$s = 2l_1(l_2\cos(\theta_3) + l_3\cos(2\theta_3) + l_4\cos(3\theta_3) + l_5\cos(4\theta_3)) + 2l_3l_4\cos(\theta_3) + 2l_3l_5\cos(2\theta_3) + 2l_4l_5\cos(\theta_3) + 2l_2(l_3\cos(\theta_3) + l_4\cos(2\theta_3) + l_5\cos(3\theta_3)) + l_1^2 + l_2^2 + l_3^2 + l_4^2 + l_5^2. \quad (42)$$

It is very obvious that the minimum and maximum reach of the end-effector of the manipulator does not depend on the first and the second angles. To determine the joint angle (θ_3), which moves the manipulator to its minimum and maximum reach, we find

$$\frac{ds}{d\theta_3} = 0 \quad (43)$$

$$-2l_3l_4\sin(\theta_3) - 2l_5l_4\sin(\theta_3) - 4l_3l_5\sin(2\theta_3) + 2l_2(l_3(-\sin(\theta_3)) - 2l_4\sin(2\theta_3) - 3l_5\sin(3\theta_3)) + 2l_1(l_2(-\sin(\theta_3)) - 2l_3\sin(2\theta_3) - 3l_4\sin(3\theta_3) - 4l_5\sin(4\theta_3)) = 0. \quad (44)$$

Using the proposed manipulator with its links length ($l_1 = 19, l_2 = 18, l_3 = 17, l_4 = 16$, and $l_5 = 15$), we get ($0 \le \theta_3 \le 72.277$). This means that the end-effector of the manipulator reaches its minimum value when ($\theta_3 = 72.277$), and reaches its maximum value when ($\theta_3 = 0$). Fig. 8 shows the manipulability value of the proposed manipulator within the joint angles' range ($0 \le \theta_2 \le \pi$) and ($0 \le \theta_3 \le 72.277$).

It is noted from this figure that the manipulability index have very good values, which are greater than zero in most of the areas of the workspace, and it is also apparent that the closer the joint angles are from the zero value, the closer the manipulability index are from singularity. This type of singularity is called boundary singularities. It is also obvious that every manipulator must have singular configurations, i.e. the existence of singularities (boundary singularities) cannot be eliminated, even by careful design.

3. Kinematics of PUMA arm

The PUMA (Programmable Universal Machine for Assembly) robot is a six-degree of freedom industrial robot, and is most commonly used in automated spot welding applications and cars assembly. It is the most common robot in university laboratories and one of the most common assembly robots.

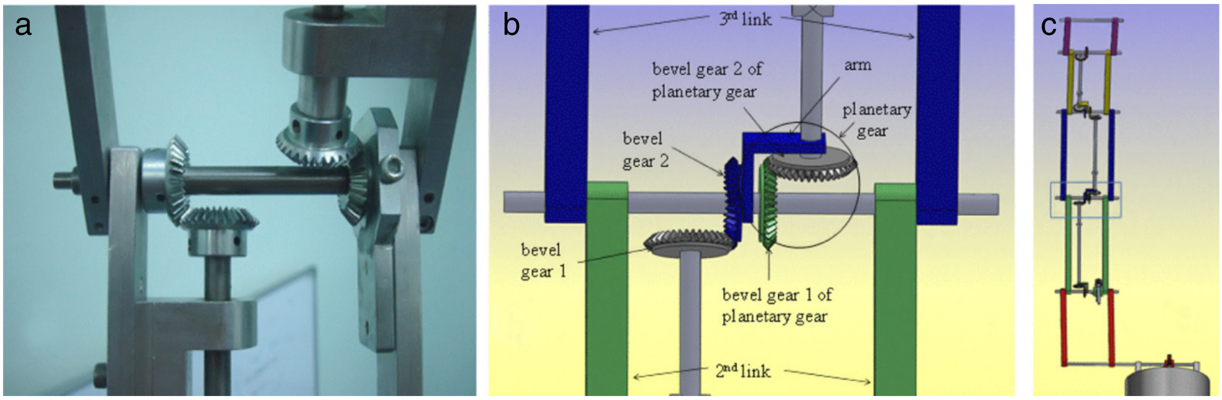

Fig. 7. The design of the fourth joint angle (third link) of the manipulator. (a) The mechanical design of the fourth joint angle; (b) the draft of the fourth joint angle using the SolidWorks software; (c) the draft of the entire manipulator using the SolidWorks software.

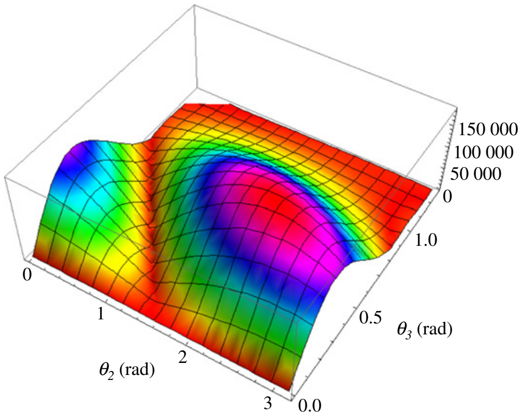

Fig. 8. The manipulability index value in whole the workspace of the proposed manipulator.

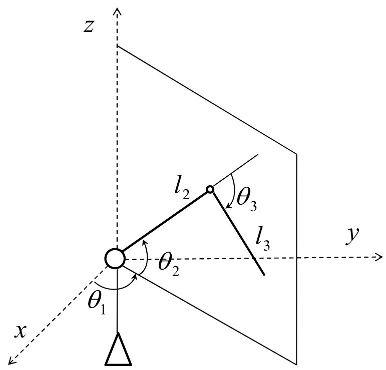

Fig. 9. PUMA arm configuration.

The proposed manipulator can be used instead of the first three degrees of freedom of the PUMA manipulator in the same application since both have three motors to control the manipulator; in other words, the proposed manipulator can be used for the same applications of the PUMA manipulator by adding the 3-*R* wrist. However, only the main three joints shown in Fig. 9 are being considered.

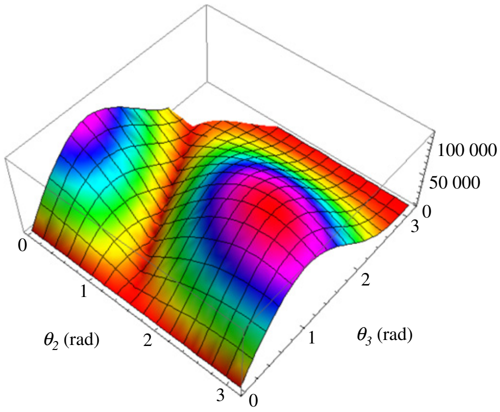

Fig. 10. The manipulability index value in whole the workspace of PUMA arm.

Using the PUMA arm of [18,19], which is shown in Fig. 9. The position equations of this arm are:

$$x = \cos[\theta_1](l_2 \cos[\theta_2] + l_3 \cos[\theta_2 + \theta_3]) \tag{45}$$

$$y = \sin[\theta_1](l_2 \cos[\theta_2] + l_3 \cos[\theta_2 + \theta_3]) \tag{46}$$

$$z = l_2 \sin[\theta_2] + l_3 \sin[\theta_2 + \theta_3]. \tag{47}$$

The Jacobian matrix for this case is given by:

$$J = \begin{bmatrix} -\mathrm{Sin}[\theta_1](l_2\mathrm{Cos}[\theta_2] + l_3\mathrm{Cos}[\theta_2+\theta_3]) & -\mathrm{Cos}[\theta_1](l_2\mathrm{Sin}[\theta_2] + l_3\mathrm{Sin}[\theta_2+\theta_3]) & -\mathrm{Cos}[\theta_1]l_3\mathrm{Sin}[\theta_2+\theta_3] \\ \mathrm{Cos}[\theta_1](l_2\mathrm{Cos}[\theta_2] + l_3\mathrm{Cos}[\theta_2+\theta_3]) & -\mathrm{Sin}[\theta_1](l_2\mathrm{Sin}[\theta_2] + l_3\mathrm{Sin}[\theta_2+\theta_3]) & -\mathrm{Sin}[\theta_1]l_3\mathrm{Sin}[\theta_2+\theta_3] \\ 0 & l_2\mathrm{Cos}[\theta_2] + l_3\mathrm{Cos}[\theta_2+\theta_3] & l_3\mathrm{Cos}[\theta_2+\theta_3] \end{bmatrix}. \tag{48}$$

To calculate the manipulability measure for PUMA arm, due to it being a non-redundant manipulator, ($m = n$) [19], Eq. (18) reduces to:

$$M = |\det(J)| \tag{49}$$

and this leads to:

$$M = |l_2 l_3 \sin(\theta_3)(l_2 \cos(\theta_2) + l_3 \cos(\theta_2 + \theta_3))|. \tag{50}$$

It is noted again that the first joint angle does not affect the value of the manipulability index. For a better comparison between the results of manipulability values for the proposed manipulator and the PUMA arm, both manipulators should have the same maximum reach, meaning that the total links length of the PUMA arm should be equal to the total links length of the proposed manipulator ($19 + 18 + 17 + 16 + 15 = 85$ cm). For PUMA arm, the manipulability measure attains its maximum when $l_1 = l_2$) for any given θ_1 and θ_2 [18,19]. This means that we will get the maximum values of manipulability when ($l_1 = l_2 = 42.5$ cm). Fig. 10 shows the manipulability value of the PUMA arm when the joint angle's range are ($0 \le \theta_2 \le \pi$) and ($0 \le \theta_3 \le \pi$).

It is noted from Figs. 8 and 10 that better results for manipulability can be obtained by using the proposed manipulator. In Fig. 8, the peak of the manipulability measure is 185 415 when $\theta_2 = 2.318$ rad, and $\theta_3 = 0.439$ rad, while the peak in Fig. 10 is 118 188 when $\theta_2 = 2.526$ rad and $\theta_3 = 1.230$ rad, which proves that the proposed manipulator can be used to improve the manipulability measure.

4. Simulation results

Demonstrating the effectiveness of the proposed method in a three dimensional manipulator, the same manipulator of Fig. 3, with the lengths of links $1 = [19, 18, 17, 16, 15]^T$ is shown in this case, with the lengths measured in cm. The goal is to move the end-effector on the path defined as:

$$x = 15 \sin(t) + 20 \tag{51}$$

$$y = 10 \cos(t) + 30 \tag{52}$$

$$z = 5 \cos(t) + 8. \tag{53}$$

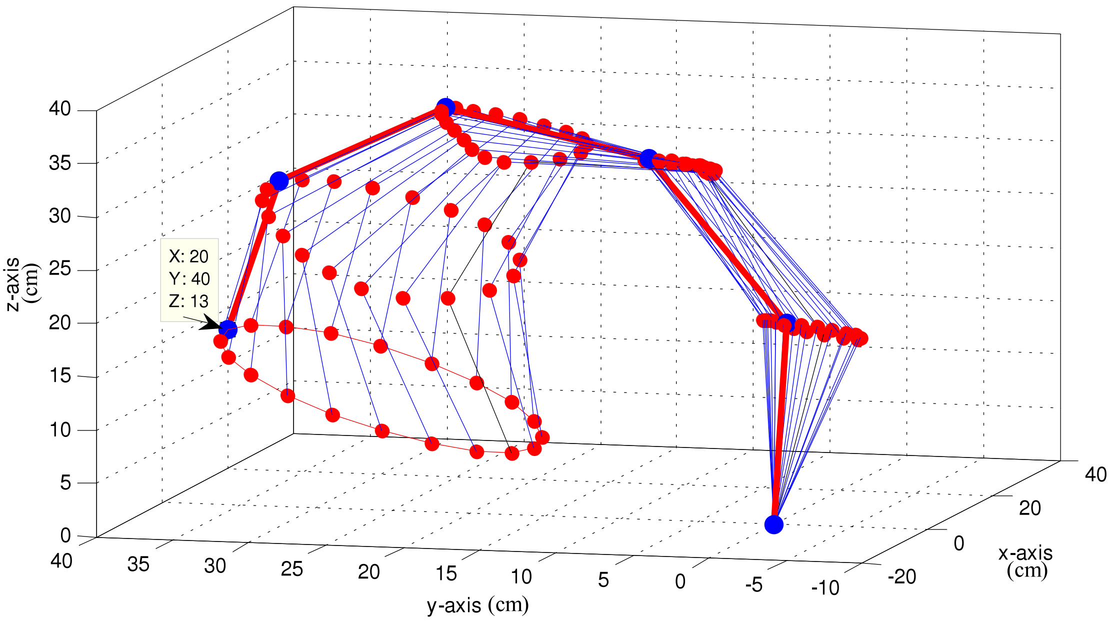

Fig. 11. The configuration of the proposed manipulator when the end-effector following the desired path.

Table 1
The angles (θ_1, θ_2, and θ_3), the singular values (σ_1, σ_2, and σ_3) and the manipulability using the proposed manipulator.

	xt	*yt*	*zt*	θ_1	θ_2	θ_3	σ_1	σ_2	σ_3	Manip
1	20.0000	40.0000	13.0000	63.4349	86.9009	41.7154	76.0249	44.7213	34.2755	116 534
2	24.6353	39.5106	12.7553	58.0560	89.6960	40.6166	78.0117	46.5622	34.0107	123 540
3	28.8168	38.0902	12.0451	52.8910	88.0268	39.9802	79.16	46.8204	33.8354	125 404
4	32.1353	35.8779	10.9389	48.1497	86.5144	39.8923	79.3184	46.4826	33.8099	124 655
5	34.2658	33.0902	9.5451	44.0001	85.9709	40.4194	78.3678	45.8268	33.958	121 955
6	35.0000	30.0000	8.0000	40.6013	86.4968	41.5771	76.2752	44.7787	34.2448	116 963
7	34.2658	26.9098	6.4549	38.1434	88.0862	43.3282	73.1071	43.0402	34.5752	108 793
8	32.1353	24.1221	5.0611	36.8934	89.3935	45.5645	69.0828	40.1815	34.809	966 24.5
9	28.8168	21.9098	3.9549	37.2462	86.1587	48.1190	64.5662	36.2006	34.8036	813 47.6
10	24.6353	20.4894	3.2447	39.7506	82.4998	50.7470	60.0806	34.4745	32.0421	663 67.2
11	20.0000	20.0000	3.0000	45	78.7586	53.1072	56.2604	33.88	28.2835	539 11.3
12	15.3647	20.4894	3.2447	53.1343	75.3234	54.7690	53.7247	33.2839	25.6101	457 95.3
13	11.1832	21.9098	3.9549	62.9593	72.6697	55.3421	52.8843	33.0439	24.5991	429 87.0
14	7.8647	24.1221	5.0611	71.9421	71.3102	54.7330	53.7781	33.2984	25.3717	454 33.7
15	5.7342	26.9098	6.4549	77.9708	71.4496	53.2210	56.0824	33.8439	27.5145	522 23.8
16	5.0000	30.0000	8.0000	80.5377	72.8291	51.2208	59.2957	34.3784	30.4138	619 98.1
17	5.7342	33.0902	9.5451	80.1688	75.0357	49.0565	62.9431	34.725	33.5836	734 03.7
18	7.8647	35.8779	10.9389	77.6359	77.7404	46.9267	66.6597	36.7302	34.8434	853 11.4
19	11.1832	38.0902	12.0451	73.6379	80.7280	44.9453	70.1926	39.6971	34.7659	968 73.2
20	15.3647	39.5106	12.7553	68.7502	83.8410	43.1842	73.3674	42.3934	34.5528	107 469.

Fig. 11 illustrates the configurations of the manipulator when the end-effector is following the desired path. The angles (θ_1, θ_2, and θ_3) have been calculated for both the manipulator, and the singular values (σ_1, σ_2, and σ_3) of J of the manipulators, and the manipulability values have also been calculated for both manipulators to show how far from the singularity the manipulator is. Tables 1 and 2 show the angles (θ_1, θ_2, and θ_3), the singular values (σ_1, σ_2, and σ_3), and the manipulability of the manipulators at all points on the desired path.

Fig. 12 shows the values of joint angles for the proposed manipulator, while Fig. 13 shows the values of joints angles for Puma arm when they follow the points on the target path.

As mentioned earlier, the bigger the dimensions of the ellipsoid are, the farther the manipulator will be from its singularity avoidance. As long as the dimensions of the ellipsoid depend on the singular values (σ_1, σ_2, and σ_3) of J of the manipulators, Tables 1 and 2 show the effectiveness of the proposed manipulator for increasing the values of (σ_1, σ_2, and σ_3), which drives the manipulator far from its singularity configurations. Fig. 14 shows the values of (σ_1, σ_2, and σ_3), using both manipulators to demonstrate how the proposed manipulator can increase the singular values of J, while Fig. 15 shows the manipulability ellipsoids of both manipulators on the desired points.

Because the manipulability measure Eq. (18) is equal to ($M = \sigma_1\sigma_2\sigma_3$) as well, using the proposed manipulator leads to an increase in the value of manipulability, which grants the capability of controlling the manipulator far from its singularity

Table 2
The angles (θ_1, θ_2, and θ_3), the singular values (σ_1, σ_2, and σ_3) and the manipulability using PUMA arm.

	xt	*yt*	*zt*	θ_1	θ_2	θ_3	σ_1	σ_2	σ_3	Manip
1	20.0000	40.0000	13.0000	63.4349	72.9842	113.5512	55.563	29.8003	29.7868	493 20.9
2	24.6353	39.5106	12.7553	58.0560	70.7114	110.7828	57.1223	29.5633	28.4467	480 38.5
3	28.8168	38.0902	12.0451	52.8910	68.7391	109.1700	58.0376	29.3963	27.0606	461 67.8
4	32.1353	35.8779	10.9389	48.1497	67.2689	108.9468	58.1645	29.3716	25.985	443 92.5
5	34.2658	33.0902	9.5451	44.0001	66.4720	110.2824	57.4059	29.5136	25.466	431 45.8
6	35.0000	30.0000	8.0000	40.6013	66.4481	113.2056	55.7566	29.7744	25.5171	423 61.4
7	34.2658	26.9098	6.4549	38.1434	67.2170	117.5796	53.3424	30.0137	25.8934	414 55.4
8	32.1353	24.1221	5.0611	36.8934	68.7245	123.0912	50.4727	29.9822	26.1782	396 15
9	28.8168	21.9098	3.9549	37.2462	70.8675	129.2652	47.6588	29.3428	25.9736	363 22.6
10	24.6353	20.4894	3.2447	39.7506	73.5162	135.4680	45.4685	27.8596	25.1179	318 17.8
11	20.0000	20.0000	3.0000	45	76.5047	140.9004	44.1554	25.7986	23.8423	271 59.9
12	15.3647	20.4894	3.2447	53.1343	79.5410	144.6408	43.5487	24.0025	22.763	237 93.7
13	11.1832	21.9098	3.9549	62.9593	82.0894	145.9116	43.3888	23.3321	22.5883	228 67.3
14	7.8647	24.1221	5.0611	71.9421	83.5601	144.5580	43.5599	24.0452	23.606	247 25.1
15	5.7342	26.9098	6.4549	77.9708	83.7829	141.1596	44.1061	25.6834	25.4796	288 63.2
16	5.0000	30.0000	8.0000	80.5377	83.0220	136.5696	45.1569	27.5875	27.4985	342 56.8
17	5.7342	33.0902	9.5451	80.1688	81.6149	131.4972	46.7879	29.4005	28.9148	397 74.8
18	7.8647	35.8779	10.9389	77.6359	79.7844	126.3996	48.8984	30.6012	29.732	444 89.5
19	11.1832	38.0902	12.0451	73.6379	77.6648	121.5720	51.2375	31.0477	30.0345	477 79.1
20	15.3647	39.5106	12.7553	68.7502	75.3572	117.2232	53.5357	30.736	30.0019	493 67.3

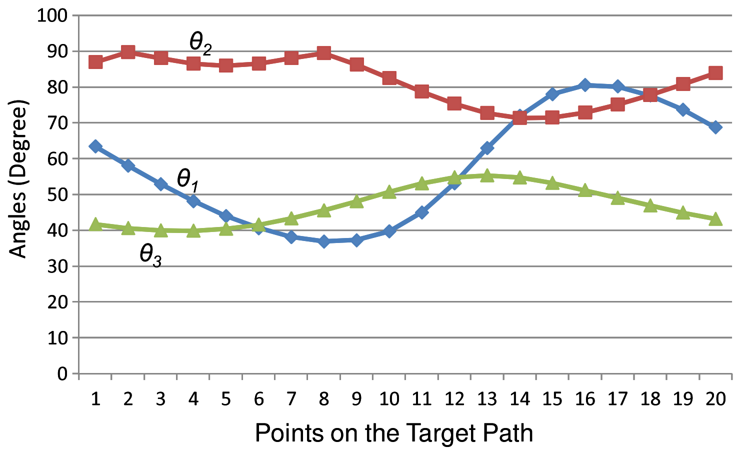

Fig. 12. The values of joint angles for the proposed manipulator when the end-effector following the desired path.

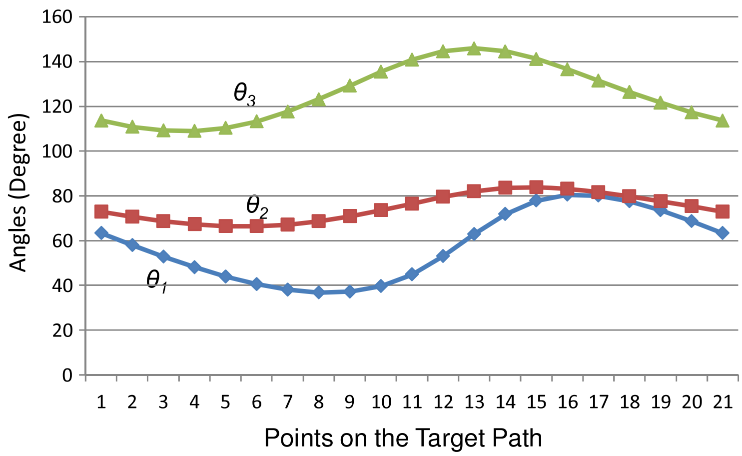

Fig. 13. The values of joint angles for Puma arm when the end-effector following the desired path.

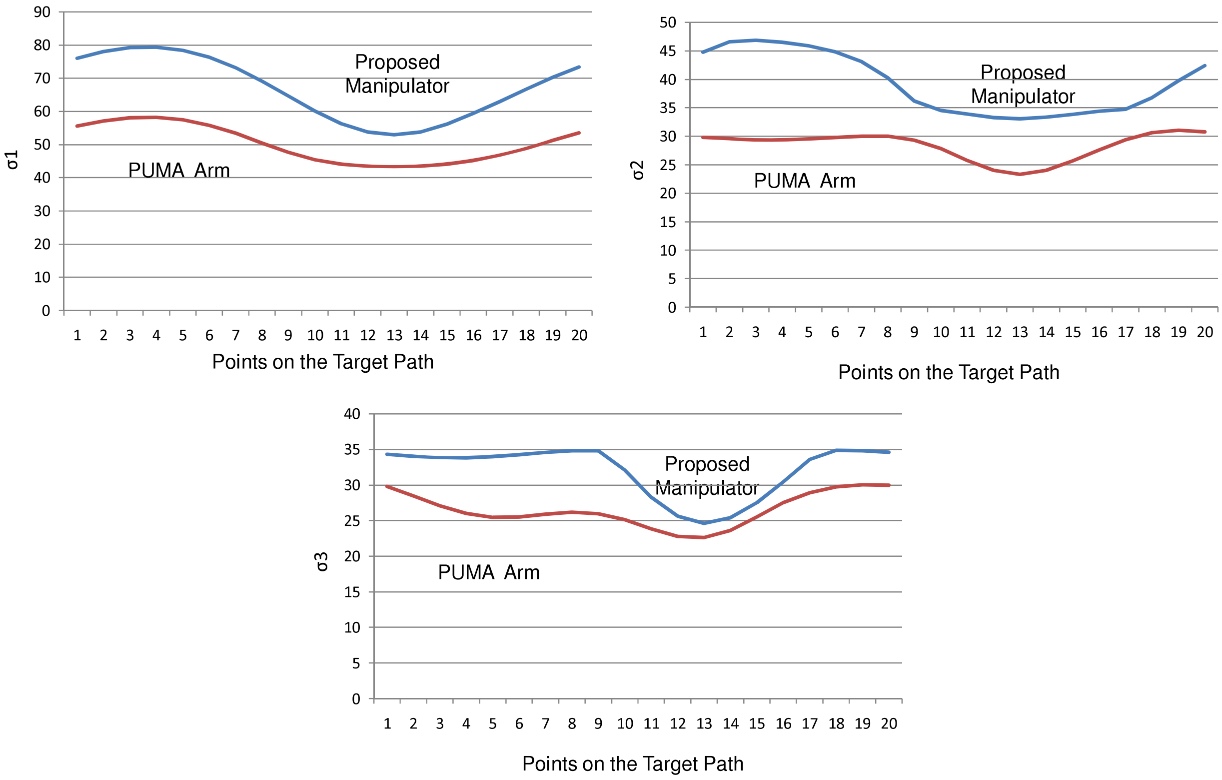

Fig. 14. The values of (σ_1, σ_2, and σ_3), the singular values of J for both manipulators.

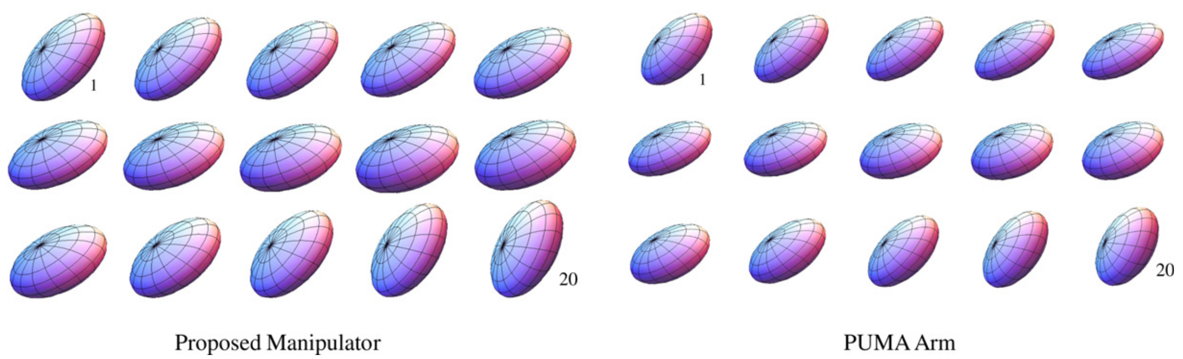

Fig. 15. Manipulability ellipsoid for both manipulators.

configurations. The values of the manipulability measure for both manipulators can be checked in Tables 1 and 2. These values are shown in Fig. 16.

5. Conclusion

The singularity avoidance of a three dimensional planar redundant manipulator has been studied in this paper. The paper proposed a method to increase the singularity avoidance ability of a three dimensional planar manipulator, by way of increasing its degrees of freedom. It is also possible to increase the degrees of freedom of the planar manipulator using the same number of motors, in order to increase the value of the manipulability measure. The manipulability ellipsoids for the proposed manipulator have been obtained and compared with the ellipsoids of the PUMA arm. The manipulability measure values of both manipulators (proposed manipulator and PUMA arm) have been calculated and analyzed, and the results of the illustrated examples show the ability of the proposed manipulator to be used exclusively for singularity avoidance.

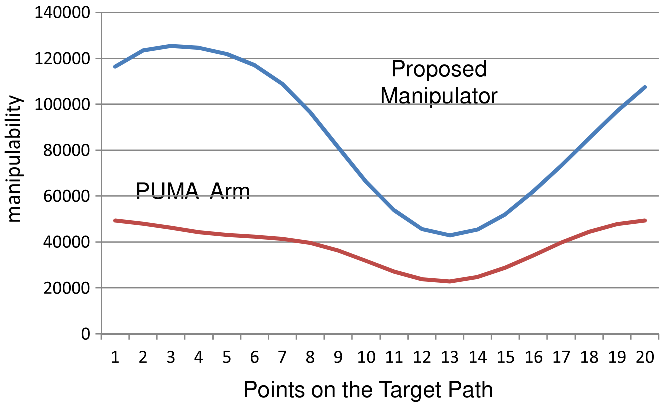

Fig. 16. Manipulability measure values for both manipulators.

References

[1] S. Yahya, H. Mohamed, M. Moghavvemi, S.S. Yang, A geometrical inverse kinematics method for hyper-redundant manipulators, in: IEEE 10th International Conference on Control, Automation, Robotics and Vision, ICARCV 2008, pp. 1954–1958.

[2] Maria da Graça Marcos, J.A. Tenreiro Machado, T.P. Azevedo-Perdicoulis, A fractional approach for the motion planning of redundant and hyper-redundant manipulators, Signal Processing 91 (2011) 562–570.

[3] M.V. Kircanski, T.M. Petrovic, Inverse kinematic solution for a 7 DOF robot with minimal computational complexity and singularity avoidance, in: IEEE International Conference on Robotics and Automation, vol. 3, 1991, pp. 2664–2669.

[4] M. Maria da Graça, B.M.D. Fernando, J.A. Tenreiro Machado, Fractional dynamics in the trajectory control of redundant manipulators, Communications in Nonlinear Science and Numerical Simulation 13 (9) (2008) 1836–1844.

[5] Ekta Singla, Suryamani Tripathi, Venkataramani Rakesh, Bhaskar Dasgupta, Dimensional synthesis of kinematically redundant serial manipulators for cluttered environments, Robotics and Autonomous Systems 58 (2010) 585–595.

[6] Liguo Huo, Luc Baron, The self-adaptation of weights for joint-limits and singularity avoidances of functionally redundant robotic-task, Robotics and Computer-Integrated Manufacturing 27 (2011) 367–376.

[7] L. Beiner, Singularity avoidance for articulated robots, Robotics and Autonomous Systems 20 (9) (1997) 39–47.

[8] A. Albert, Regression and the Moore–Penrose Pseudo-Inverse, Academic Press, New York, 1972.

[9] D.E. Whitney, Resolved motion rate control of manipulators and human prostheses, IEEE Transactions on Man–Machine Systems MMS-10 (2) (1969) 47–53.

[10] W. Khalil, E. Dombre, Modeling, Identification and Control of Robots, Hermes Penton Ltd., 2002.

[11] J. Baillieul, Kinematic programming alternatives for redundant manipulators, in: IEEE International Conference on Robotics and Automation, 1985, pp. 722–728.

[12] C.A. Klein, C. Huang, Review of pseudo inverse control for use with kinematically redundant manipulators, IEEE Transactions on Systems, Man, and Cybernetics SMC-13 (2) (1983) 245–250.

[13] A. Liegeois, Automatic supervisory control of the configuration and behaviour of multibody mechanisms, IEEE Transactions on Systems, Man, and Cybernetics SMC-17 (1) (1977) 868–878.

[14] H.P. Singh, N. Sukavanam, Neural network based control scheme for redundant robot manipulators subject to multiple self-motion criteria, Mathematical and Computer Modelling 55 (3–4) (2012) 1275–1300.

[15] Naveen Kumar, Vikas Panwar, N. Sukavanam, S.P. Sharma, J.H. Borm, Neural network-based nonlinear tracking control of kinematically redundant robot manipulators, Mathematical and Computer Modelling 53 (2011) 1889–1901.

[16] T. Yoshikawa, Analysis and control of robot manipulators with redundancy, in: Robotics Research: The First International Symposium, MIT Press, 1984, pp. 735–747.

[17] T. Yoshikawa, Manipulability of robotic mechanisms, The International Journal of Robotics Research 4 (2) (1985) MIT Press, Cambridge, MA.

[18] T. Yoshikawa, Manipulability and redundancy control of robotic mechanisms, in: International Conference on Robotics and Automation, 1985, pp. 1004–1009.

[19] T. Yoshikawa, Foundations of Robotics: Analysis and Control, The MIT Press, 1990.

[20] Samer Yahya, M. Moghavvemi, Haider A.F. Mohamed, Geometrical approach of planar hyper-redundant manipulators: inverse kinematics, path planning and workspace, Simulation Modelling Practice and Theory 19 (1) (2011) 406–422.